INTERFACE

rsif.royalsocietypublishing.org

Research

Cite this article: Soomro A, Alsop RJ, Negishi A, Kreplak L, Fudge D, Kuczmarski ER, Goldman RD, Rheinstädter MC. 2017 Giant axonal neuropathy alters the structure of keratin intermediate filaments in human hair. *J. R. Soc. Interface* **14**: 20170123. http://dx.doi.org/10.1098/rsif.2017.0123

Received: 18 February 2017
Accepted: 24 March 2017

Subject Category:
Life Sciences–Physics interface

Subject Areas:
biomaterials, biophysics

Keywords:
giant axonal neuropathy, human hair, keratin intermediate filaments, X-ray diffraction, tensile testing

Author for correspondence:
Maikel C. Rheinstädter
email: rheinstadter@mcmaster.ca

Electronic supplementary material is available online at https://dx.doi.org/10.6084/m9.figshare.c.3734386.

THE ROYAL SOCIETY PUBLISHING

Giant axonal neuropathy alters the structure of keratin intermediate filaments in human hair

Asfia Soomro[1], Richard J. Alsop[1], Atsuko Negishi[2], Laurent Kreplak[3], Douglas Fudge[2], Edward R. Kuczmarski[4], Robert D. Goldman[4] and Maikel C. Rheinstädter[1]

[1]Department of Physics and Astronomy, McMaster University, Hamilton, Ontario, Canada
[2]Department of Integrative Biology, University of Guelph, Guelph, Ontario, Canada
[3]Department of Physics and Atmospheric Science, Dalhousie University, Halifax, Nova Scotia, Canada
[4]Department of Cell and Molecular Biology, Northwestern University, Chicago, IL, USA

MCR, 0000-0002-0558-7475

Giant axonal neuropathy (GAN) follows an autosomal recessive genetic inheritance and impedes the peripheral and central nervous system due to axonal swellings that are packed with neurofilaments. The patients display a number of phenotypes, including hypotonia, muscle weakness, decreased reflexes, ataxia, seizures, intellectual disability, pale skin and often curled hair. We used X-ray diffraction and tensile testing to determine potential changes to the structure of keratin intermediate filaments (IFs) in the hair of patients with GAN. A statistically significant decrease in the 47 and the 27 Å diffraction signals were observed. Tensile tests determined that the hair was slightly stiffer, stronger and more extensible in GAN patients. These results suggest that the structure of keratin IFs in hair is altered in GAN, and the findings are compatible with an increased positional disorder of the keratin tetramers within the hair fibres.

1. Introduction

Giant axonal neuropathy (GAN) is a rare paediatric neurodegenerative disease that is autosomal recessive. Patients usually present with a number of phenotypes ranging from hypotonia, muscle weakness, decreased reflexes, ataxia, seizures, intellectual disability, pale skin and often tightly curled hair [1,2]. The underlying pathology originates from the accumulation of intermediate filaments (IF) in Schwann cells, fibroblasts, melanocytes, endothelial and Langerhans cells, as well as axonal swellings filled with neurofilaments [1].

GAN is a disease known to affect several types of IFs [2]. The recessive mutation in the GAN gene results in the destabilization and degradation of gigaxonin proteins. The physiological role of gigaxonin is the regulation and clearance of IFs. Gigaxonin is an E3 ligase adaptor protein involved in the degradation of IF via the ubiquitin–proteasomal system. Therefore, GAN is believed to be the result of failed clearance of excess IFs leading to harmful deposits that cause axonal swelling and degradation [2].

A common symptom of GAN is curly, frizzy hair. The cortex comprises most of the hair fibre and is primarily composed of keratin proteins and structural lipids. The keratin protein is an α-helical protein, which forms coiled-coil dimers in strands along the fibre axis. Keratin IFs are composed of 26–34 chains [3]. In a simple model, one tetramer (consisting of two keratin coiled-coils dimers) in the centre is surrounded by six other tetramers, (seven tetramers and 28 chains) to form bundles 75–90 Å in size [4–6], as shown in figure 1*a*).

Using X-ray diffraction and tensile testing, we compared scalp hair from GAN patients with hair from their normal parents as controls. The results present evidence that GAN, in addition to influencing filament accumulation, also alters the structure of keratin IFs within human hair.

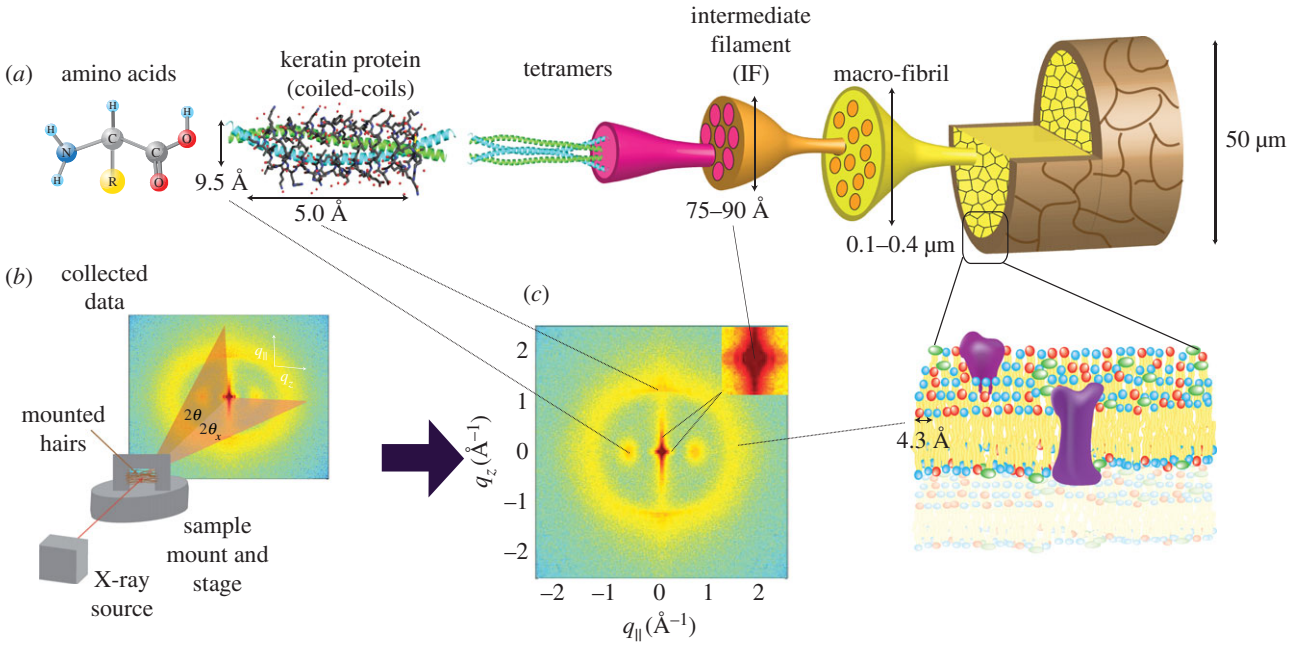

Figure 1. Illustration of the structure of hair. (*a*) Molecular cartoons of the hierarchic organization of hair from keratin coiled-coil dimers to intermediate filaments and fibrils including lipids in the cell membrane complex. In intermediate filaments, one tetramer (consisting of two keratin coiled-coils dimers) in the centre is surrounded by six tetramers, (seven tetramers and 28 chains) to form bundles 75–90 Å in size. (*b*) Schematic of the X-ray setup: hair strands were mounted and aligned on the diffractometer. (*c*) Two-dimensional X-ray data were measured for each specimen covering distances from about 3 Å up to 250 Å including signals from the coiled-coil α-keratin phase, the keratin IFs in the cortex, and from lipids in the membrane complex.

2. Results

Hair samples were obtained from six families from Belgium, Germany, New Zealand, and the US (New York City, Tampa Bay and Ohio), with a total of 17 subjects, as listed in table 1. A set of ~30 hair strands per subject was used in the diffraction experiments, while single hairs were probed in the tensile tests. The families probably followed standard Western hygiene practices, using shampoo and conditioner on a regular basis; consequently, the hairs cannot be considered 'virgin hairs' [7]. However, shampoo and conditioner were recently shown not to have an effect on molecular hair structure [8].

With respect to the physical appearance of the hair samples, five out of six patients presented with very curly and frizzy hair, in agreement with previous reports on the description of GAN patients' hair texture. The hair sample from the New Zealand patient appeared normal, with no obvious deformities. Visual descriptions of the hair are listed in table 1.

2.1. X-ray diffraction analysis

A schematic of a typical diffraction set-up is shown in figure 1*b*. The hair strands were mounted and oriented on the diffractometer to measure structure along, and perpendicular to the hair separately but simultaneously. The result of such a diffraction experiment is a two-dimensional intensity map, as shown in figure 1*c*. The different signals can be assigned to packing of keratin proteins in coiled-coils and IFs, as well as lipids in the membrane complex, as indicated in the cartoons.

Two-dimensional X-ray intensity maps collected for the Ohio family are displayed in figure 2 as examples. Because of GAN's recessive inheritance pattern, both heterozygous parents were disease-free, and were used as controls. The hair strands were oriented, such that their long axis was parallel with the vertical *z*-axis. The displayed (q_z, $q_{||}$)-range covers the features of interest, as described in the Material and methods section, and these maps exhibit the characteristic features reported previously [8–10].

A number of peaks were observed and the assignment of scattering signals to the corresponding biological structures is depicted in figure 1. The keratin proteins in the cortex are known to organize in bundles, whose structure is dominated by α-helical coiled-coils [9,11]. Coiled-coils consist of α-helices that wind together to form a rope-like structure stabilized by hydrophobic interactions. The coiled-coil motif is found in about 10% of the proteins in the human genome [12].

The coiled-coil motif's structure is shown by a ~9.8 Å ($q_{||} \sim 0.66$ Å^{-1}) equatorial reflection corresponding to the spacing between the constituent α-helical chains and a ~5.0 Å meridional reflection ($q_z \sim 1.25$ Å^{-1}) arising from the super-helical structure of α-helices twisting around each other within coiled-coils [13–15]. In addition, a broad ring of scattering is observed at $|q| \sim 1.6$ Å^{-1} as a result of the lipid order within the membrane complexes.

To quantitatively analyse potential changes in the molecular structure of the hair, the two-dimensional data were integrated along the $q_{||}$ and q_z directions and converted into line scans. Corresponding wide-angle X-ray scattering (WAXS) and small-angle X-ray scattering (SAXS) data are displayed in figures 3 and 4.

Signals observed in the wide angle region along the $q_{||}$ and q_z axis in figure 3 are related to packing of keratin molecules into coiled coils, as well as lipids in the cell membrane complex. Data were fit by a series of Lorentzian peak profiles modelling the structure of keratin proteins and membranes for Ohio father (a) and (d), Ohio mother (b) and (e), and the Ohio patient in (c) and (f). All fitting parameters are listed in electronic supplementary material, table S1. No statistically significant differences were observed

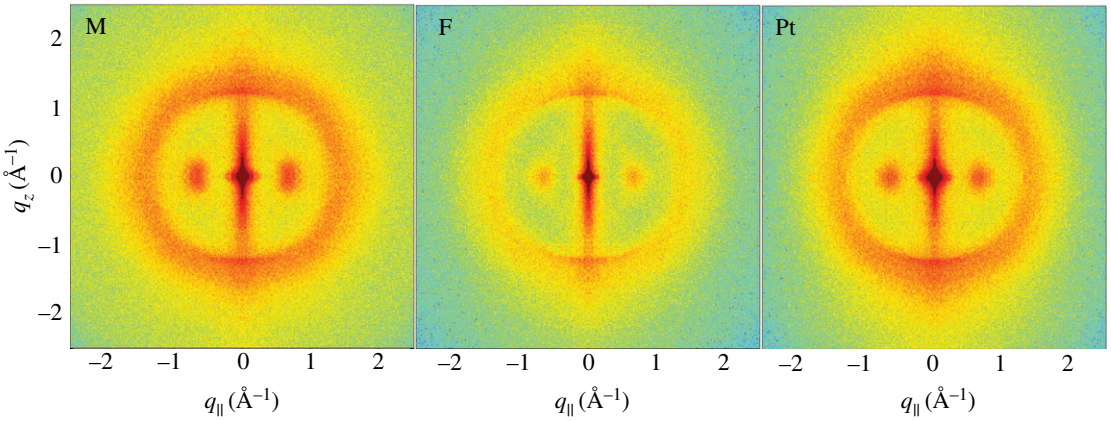

Figure 2. Two-dimensional X-ray diffraction images from hair samples of the Ohio family. The hair strands were oriented with the long axis of the hair parallel with the vertical *z*-axis. The displayed (q_z, $q_{||}$) range covered length scales from 3 Å up to 250 Å to study the coiled-coil α-keratins, keratin IFs, as well as lipids in the membrane layer in the cortex [8,9]. The features observed are common among the individuals in this study, and agree well with previous reports. The labels 'M', 'F' and 'Pt' refer to mother, father and patient, respectively. (Online version in colour.)

Table 1. List and description of all hair samples included in this study. Physical appearance of each individual's hair, length of strands, relationship between the subjects. No prior knowledge of age, ethnicity or daily hair care regimen was provided. Number of strands used for the X-ray diffraction experiments are given. Single hair strands were used for the tensile experiments. Hair samples that are italicized represent that an insufficient number of strands were obtained to perform X-ray diffraction experiments. These samples are, therefore, included in the tensile analysis, only.

GAN samples	individual	colour	straight/curly	sample number	# of strands	hair length
New York	patient	brown	curly	1	50	short
	mother	golden	straight	2	30	short
	father	black	straight	3	3	short
Ohio	patient	black	curly	4	200	short
	mother	black	straight	5	30	short
	father	black	straight	6	50	short
Florida	*patient*	black	curly	7	2	short
	mother	black	straight	8	100	short
	father	black	straight	9	60	short
Belgium	patient	red/brown	curly	10	150	short
	mother	brown	straight	11	30	long
	father	brown	straight	12	100	medium
Germany	patient	black	curly	13	50	short
	mother	black	straight/wave	14	75	medium
	father	black	straight	15	75	medium
New Zealand	patient	brown	straight	16	30	short
	mother	brown	straight	17	50	long

in peak position or width between patient and the control or data published previously [8–10] indicating that the molecular structure on this length scale is not different between GAN patients and controls (within the resolution of our experiment).

In order to investigate IF structure, SAXS was performed along $q_{||}$ from $0.03\,\text{Å}^{-1} < q_{||} < 0.3\,\text{Å}^{-1}$, covering length scales of 21 Å up to 250 Å, and the resultant curves for the German and Ohio families are shown in figure 4*a*. SAXS profiles of human hair typically show peaks at 90, 47 and 27 Å (corresponding to $q_{||}$-values of ~0.07, ~0.13 and ~0.23 Å^{-1}), related to the internal structure of the keratin IFs. There was a significant decrease in intensity at 47 and 27 Å in the Ohio and German patients, when compared with their parents, while positions of the peaks were unchanged within the resolution of our experiment. SAXS data for all participants in this study are shown in electronic supplementary material, figure S1 and fitting parameters are listed in electronic supplementary material, table S2.

The intensity of the 47 and 90 Å peaks were integrated and the ratio of these integrated intensities was averaged for the patient and control groups, respectively. The results are shown in figure 4*b*. The relative intensity of the 47 Å peak in the patient group was found to be decreased by 26% when compared with the control. The 27 Å signal was not used for the analysis because, even in the controls, the peak intensity was small, with corresponding large uncertainties, which made quantitative analysis difficult.

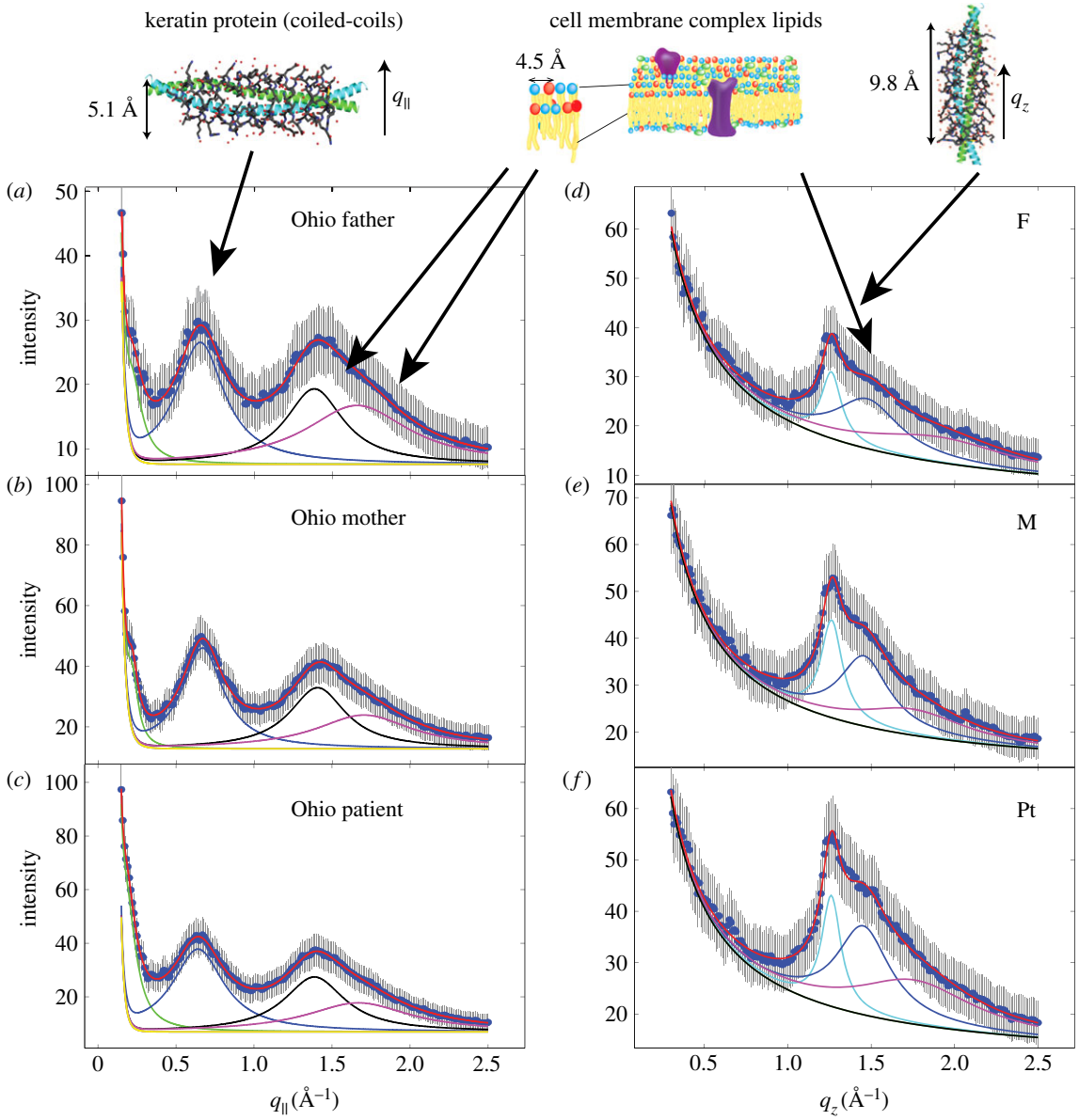

Figure 3. Wide angle X-ray scattering profiles. Panels ($a-c$) measure the structure in the plane of the hair fibres ($q_{||}$). The data are well described by five Lorentzian peak profiles with an exponential background: (i) a small angle peak observed in higher resolution in the SAXS profiles in figure 4; (ii) a peak at 9.8 Å, assigned to lateral packing of keratin coiled-coils; (iii) a lipid peak at 4.5 Å related to packing of lipid tails in the membrane complex; (iv) a peak at 3.5 Å, assigned to amorphous protein; and (v) a second order lipid peak at 2.3 Å. Data in ($d-f$) were measured along the z-axis of the hair fibres (q_z). The two signals correspond to lipids in the membrane complex and the pitch of the keratin proteins. 'M', 'F' and 'Pt' refer to mother, father and patient. No significant differences were observed in peak position or width between patient and the control, as well as data in the literature [8–10]. (Online version in colour.)

2.2. Tensile experiments of hair samples

To probe the mechanical properties of GAN hair, tensile tests were performed, as described in detail in the Material and methods section. On average, nine hair strands of each individual were measured and included in a statistical analysis, resulting in 155 total tensile measurements. In the tensile experiments, the stress (force/unit area) as a function of hair extension or strain ($\Delta\ell/\ell$) was recorded up to the point of hair fracture. Curves for the Belgium family are shown in figure 5 as examples. Raw data of all tensile experiments are provided as the electronic supplementary material.

The first linear portion of the curve is related to elastic stretching of keratin in the hair fibre, and the slope of this region is proportional to the Young's modulus of the fibre [16,17]. In addition, the stress and strain at the point of fracture were recorded. Diameter had a strong effect on Young's modulus ($p < 0.0001$) and breaking stress ($p < 0.0001$), with thinner hairs being generally stiffer and stronger than thicker ones. Diameter had no effect on breaking strain ($p = 0.370$). After accounting for diameter effects, GAN patient hair was both stiffer ($p < 0.0001$) and stronger ($p = 0.0082$) than controls. GAN patient hair was also significantly more extensible ($p = 0.012$). The results of the tensile experiments are summarized in figure 6.

3. Discussion

X-ray diffraction has long been used to reveal the molecular structure and organization of many biomaterials because it presents a non-invasive assessment [8,9,18–20]. Mechanical testing of hair provides information about stiffness and stability. By combining a microscopic and a macroscopic technique, macroscopic properties can be linked to microscopic structure.

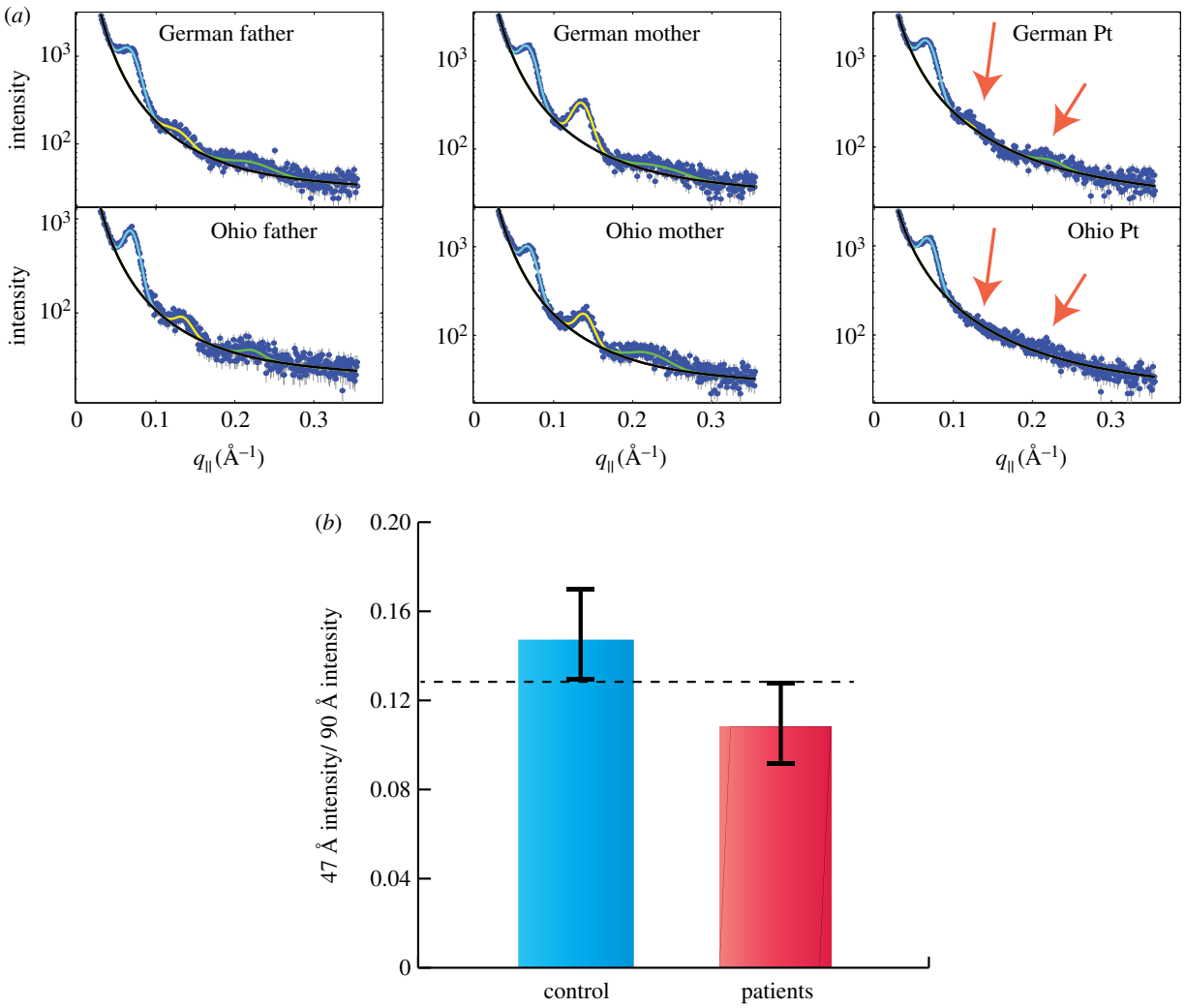

Figure 4. Small angle X-ray scattering profiles, covering length scales from 20 Å up to 250 Å. (*a*) Datasets are shown for the German and one US family (OH). Peaks were observed at 90, 47 and 27 Å (corresponding to $q_{||}$-values of ~0.07, ~0.13 and ~0.23 Å^{-1}), related to the internal structure of the keratin IFs. In all patients, the signals at 47 and 27 Å were found to be significantly decreased when compared with the control. (*b*) The bar graph depicts the ratio between integrated peak intensities at 47 and 90 Å. Following statistical analysis, there was a significant decrease in the 47 Å signal in all patients. The 27 Å signal was not included in the analysis because of the small peak intensities and corresponding large uncertainties. (Online version in colour.)

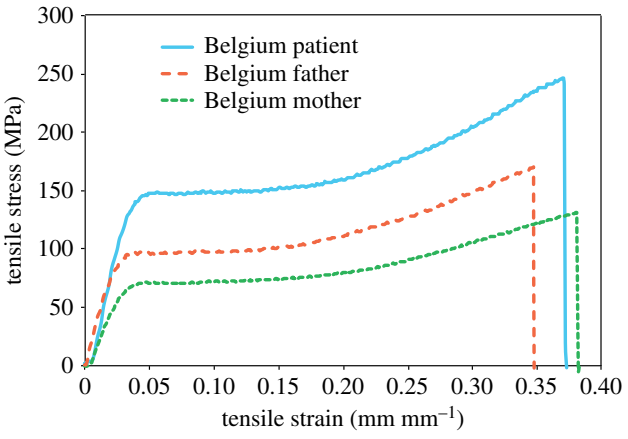

Figure 5. Exemplary tensile curves of the Belgium family. These curves are in good agreement with typical tensile experiments in human hair. The determination of elastic parameters is described in the text. (Online version in colour.)

X-ray diffraction in combination with mechanical testing was previously used to study scalp hair of a patient with a novel ribosomopathy [10]. One of the symptoms of this rare disease is that patients present with thin and brittle hair. As a consequence, the patient's hair was found to be measurably thinner and contained less lipid in relation to keratin when compared with the patient's family. In this study, we combined X-ray diffraction and tensile testing to investigate the question of whether GAN has an effect on the structure and properties of hair.

In general, WAXS measurements for all individuals in this study yielded results within normal limits, indicating that packing at the level of individual keratin molecules is unaffected by GAN. SAXS measurements, however, revealed a decrease in the 47 and 27 Å signals between the patients and their parents.

3.1. Model describing structure of the intermediate filaments

The SAXS signals observed in this experiment agree well with those reported from previous experiments. Signals in the SAXS region of 90, 47 and 27 Å along the cross-sectional direction have previously been assigned to the structure of intermediate filaments. However, the interpretation of these signals is not consistent throughout the scientific literature. Fraser & MacRae proposed a model to explain the scattering of α-keratin in 1958 [4]. The three signals can be modelled by

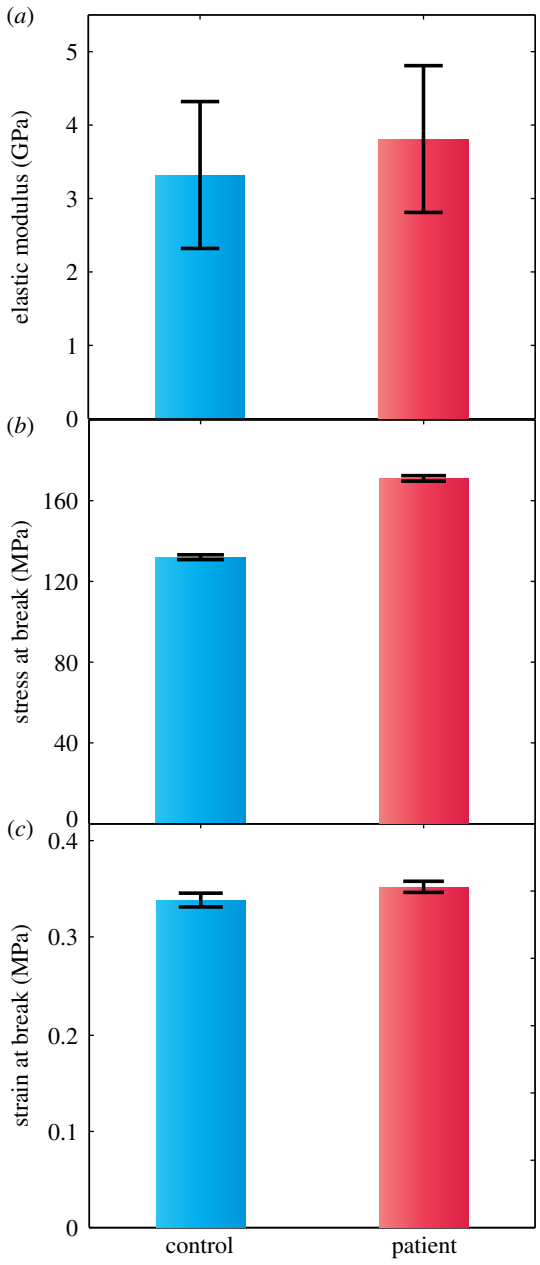

Figure 6. Results of the tensile experiments. Young's modulus (*a*), stress at break (*b*) and strain at break (*c*) as determined from statistical analysis for the control group and the patients. While the patients' hair was found to be slightly stiffer (patients 3.81 ± 1 GPa versus control 3.32 ± 1 GPa) and show a slightly increased strain at break (0.35 ± 0.01 MPa when compared with 0.33 ± 0.007 MPa), the stress at break was significantly increased from 133 ± 1 MPa to 169 ± 1 MPa. (Online version in colour.)

a cylinder of radius R embedded in a surrounding matrix with a different scattering power, as the maxima of a Bessel function. In this model, changes in the peak intensities can be attributed to changes in the matrix.

It is well established that when human hair absorbs moisture, the water mostly accumulates in the matrix leading to a displacement of the 90 Å peak to larger distances (matrix swelling) and a decrease of intensity of the 47 and 27 Å peaks due to a loss of contrast between the matrix and IF [5]. So within this scenario, the loss of intensity that we observed for the patients compared with their parents may point towards an increase in water uptake by the matrix of the patients. However, this also means that the patients' hair should have a lower Young's modulus and a lower breaking

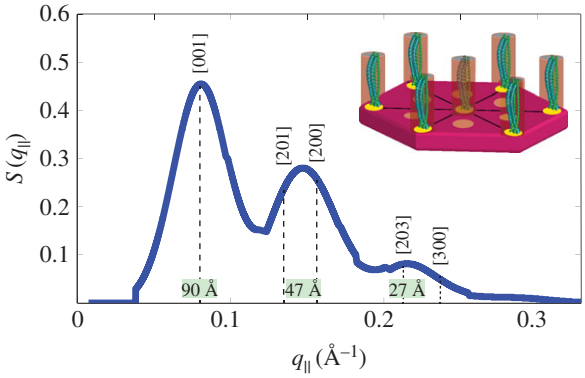

Figure 7. Calculated small angle structure factor. Keratin tetramers were modelled as packed solid cylinders within the IF. A hexagonal packing of the coiled-coil tetramers then well described the experimental small angle data. The model takes into account the experimental resolution, which leads to a broadening of the hexagonal diffraction peaks. The cartoon shows the arrangements of solid tetramer cylinders within the intermediate filament. Peaks are indexed by their hexagonal [*hkl*] reflections. (Online version in colour.)

stress than their parents because water acts as a plasticizer within hairs. As this contradicts our mechanical data and the fact that the diffraction peak positions did not change, we introduced our disordered IF model, which well describes the experimental findings.

The Fraser & MacRae model is the lowest resolution model that can reproduce the position and relative intensities of the peaks at 47 and 27 Å. However, as already stated by Fraser & MacRae in their 1958 paper, this model does not exclude the possibility that IFs consist of organized, hexagonally packed groups of α-helices. Consequently, a more detailed molecular model of the IF by Er Rafik *et al.*, which takes the keratin coiled-coils atomic structure into account, explicitly, has been shown to fit these peaks equally well [6]. In this paper, we propose an intermediate approach between the one of Fraser & MacRae, and the one of Er Rafik *et al*. We assume keratin coiled-coil tetramers are hexagonally packed solid cylinders within the IF with some degree of positional disorder.

The small angle peak pattern with peaks at 90, 47 and 27 Å is compatible with a model of seven tetramers arranged on a hexagonal lattice, as shown in figure 7. Technically, packing of the filaments was described by a primitive monoclinic unit cell, space group $P2$, with lattice constants $a = c = 90$ Å and $\alpha = 90^\circ$, $\beta = 60^\circ$ and $\gamma = 90^\circ$. The corresponding structure factor was calculated and convoluted with the instrumental resolution, which leads to a finite peak width. The result is shown in figure 7. The corresponding [*hkl*] reflections are marked in the figure. This model well reproduces the pattern of reflections and intensities at 90, 47 and 27 Å typically observed in hair.

3.2. Analysis of the X-ray diffraction in giant axonal neuropathy patients

The signals at 47 and 27 Å in SAXS were found to be significantly decreased in the patients' hair in figure 4, when compared with their parents. After normalizing the 47 Å peak intensity by the intensity of the peak at 90 Å and averaging the calculated results of the parents and patients, patients showed a 26.4% decrease in the 47 Å peak. A decrease in intensity of the higher-order peaks is compatible with an increase in positional disorder of the keratin tetramers.

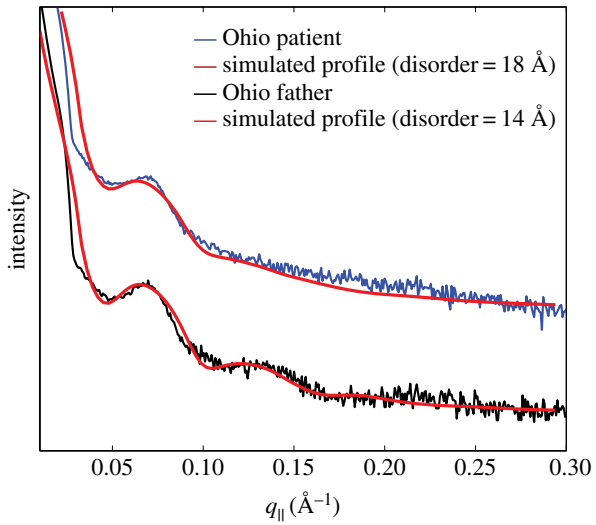

Figure 8. Fitting the structural model to the SAXS data. Scattering data of Ohio father and patient together with the fitted theoretical profiles. The red lines are fits using equation (5.1). Fits with disorder parameters of $\Delta X = 14$ Å respective 18 Å provided best agreements. (Online version in colour.)

To illustrate and quantify the effect of disorder in the position of tetrameric protofilaments on the SAXS profile, a computational model was created, where the positional disorder of a two-dimensional hexagonal cell could be explicitly varied. Details of the model are given in the Materials and methods section.

Positional disorder influences the intensity of diffraction peaks in a q-dependent manner, according to the Debye–Waller factor (DWF) [21]

$$F(q) = F_0(q)\mathrm{e}^{-\Delta X^2 q^2}, \tag{3.1}$$

where ΔX represents the average displacement of the tetramers from their ideal position in the hexagonal lattice.

The IF was modelled in two dimensions using a set of 17 hexagonally tiled cylindrical scatterers. Initially, the cylinders were arranged on a perfect hexagonal grid. Next, each point on the grid is displaced, using a value chosen randomly from a Gaussian distribution centred at zero with a width of ΔX. The above steps are performed for $0 < |\Delta X| < 40$ Å, then repeated 50 times and averaged for each ΔX. The results are shown in figure 8 using Ohio father and patient as examples. The red curves are fits after equation (5.1). The parent group in our study showed an average displacement ΔX of $\Delta X = 16$ Å ($\pm$ 0.1 Å), and the patients an average $\Delta X = 17$ Å ($\pm$ 0.1 Å).

Our tensile tests indicate greater mechanical strength in GAN hair versus control. Increased disorder within filaments also suggests decreased lateral interactions between keratin molecules. Kreplak *et al.* determined that during extension, keratin molecules within an intermediate filament physically stretch and also slide past each other, thereby breaking sulfur bonds in the process [17,22]. Our tensile tests suggest GAN hair is more extensible than the control hair, as the GAN hair reaches higher strain before fracture. This observation is in agreement with the changes in the molecular organization, as it has been reported that greater positional disorder is expected to lead to greater extensibility [23].

However, it has to be ruled out that the observed effect is potentially an age-related effect, as the control group (the parents) in this study is significantly older than the patients. Breaking force was found to decline with age, however, the hair diameter also declines with age, such that the breaking stress (calculated as breaking force divided by the cross-sectional area) remains constant [24], indicating that the effect is indeed GAN-related.

Currently, theories on the pathology of GAN suggest that mutations in the gigaxonin protein lead to an accumulation of intermediate filaments in various tissues. We present experimental evidence that keratin IFs are affected and their structure is disrupted in GAN.

4. Conclusion

GAN is a rare neurodegenerative disease associated with the aggregation of IFs and disruption of IF clearance. We studied hair of GAN patients using X-ray diffraction and tensile testing to determine potential changes to the structure of keratin IFs. Seven GAN patients and their parents were included in this study. A statistically significant decrease of the 47 and 27 Å diffraction signals was observed in patients' hair when compared with their parents' hair. From tensile tests, hair is slightly stiffer, stronger and more extensible in GAN patients. These results indicate that the structure of keratin IFs in hair is altered by GAN and are compatible with increased positional disorder of the keratin tetramers within the IF.

5. Material and methods

5.1. Obtaining hair samples

The study included 17 individuals, as listed in table 1. All individuals were included in the tensile tests and an average of nine hair strands per individual was measured, resulting in 155 total measurements. The hair samples from the Florida family members and the NYC father could not be used in the diffraction experiments due to the limited amount of hair strands available.

At the beginning of the study, a varying number of hair strands were obtained from the subject's frontal scalp region, less than 10 cm from the roots, and mailed to Hamilton and Guelph, Ontario, Canada.

5.2. Diffraction experiments

To prepare hair for diffraction analysis, hair samples were cut into strands ~3 cm long. Care was taken to prevent stretching or deforming the hair strands during this process. For each subject, approximately 30 strands were mounted onto an aluminum apparatus. The cut-out at the middle of the apparatus allows for the scattering of X-ray signals on the hair sample. The apparatus was then mounted horizontally onto the loading plate of the Biological Large Angle Diffraction Experiment (BLADE). All hair samples were scanned at ambient conditions, i.e. room temperature and humidity of 28°C and 50% RH.

X-ray diffraction data were obtained using BLADE in the Laboratory for Membrane and Protein Dynamics at McMaster University. BLADE uses a 9 kW (45 kV, 200 mA) CuKα Rigaku Smartlab rotating anode at a wavelength of 1.5418 Å. Focusing multi-layer optics provides a high-intensity parallel beam with monochromatic X-ray intensities up to 10^{10} counts (s^{-1} mm^{-2}). By aligning the hair strands in the X-ray diffractometer, the molecular structure along the fibre direction and perpendicular to the fibres could be determined. We refer to these components of the total scattering vector, $\boldsymbol{Q}$, as q_z and $q_{||}$, respectively. An illustration of q_z and $q_{||}$ orientations is shown in figure 1*b*.

The result of such an X-ray experiment is a two-dimensional intensity map of a large area of the reciprocal space of -2.5

$\text{Å}^{-1} < q_z < 2.5\ \text{Å}^{-1}$ and $-2.5\ \text{Å}^{-1} < q_{\|} < 2.5\ \text{Å}^{-1}$ (figure 1*c*). The corresponding real-space length scales are determined by $d = 2\pi/|Q|$ and cover length scales from ~2.5 to 250 Å, incorporating typical molecular dimensions and distances for primary and secondary protein structures and lipid structures.

5.3. Scattering model

The IF was modelled in two dimensions using a set of 17 hexagonally tiled cylindrical scatterers, where each scatterer, i is placed at position $r_i'(x, y)$ on a perfect hexagonal grid. Then, each scatterer is displaced by $\epsilon(x, y)$, chosen from a Gaussian distribution of width ΔX centred at zero, such that $r_i(x, y) = r_i'(x, y) + \epsilon(x, y)$.

Next, the two-dimensional structure factor $S(q_x, q_y)$ was calculated as

$$S(q_x, q_y) = \sum_i \exp(-\mathrm{i} r_i \cdot q). \tag{5.1}$$

The intensity, $I(q_x, q_y)$ was then found with $I(q_x, q_y) = |S(q_x, q_y)|^2$. The two-dimensional data were projected onto $q_{\|}$ yielding $I(q_{\|})$. Finally, a constant background which decayed as $1/q^2$ was added to agree with the background observed in the experiment.

The above steps are performed for $0 < |\Delta X| < 40$ Å, then repeated 50 times and averaged for each ΔX. Scattering profiles were generated from the model system and are shown in figure 9. As demonstrated by the results, due to the q^2 dependence in the DWF, increasing positional disorder eliminates the intensity of higher-order peaks more strongly than the lower-order peaks. Matlab code to calculate the diffraction profiles is provided as electronic supplementary material.

5.4. Tensile tests and statistical analysis

Tensile tests of individual hair strands from patients and parents were performed on an Instron single-column testing machine (model 3343, Instron, Norwood, MA, USA) with a 10 N load cell and a constant crosshead speed of 4.8 mm min^{-1}. The hair samples were fixed at their ends with Klebfix glue onto a cardstock paper frame to protect the fibre from unintentional forces and deformations during sample mounting to the testing apparatus. The nominal gauge length ranged from 3.5 to 5 mm.

Hair samples were mounted and tested at room temperature on the same day. For each mounted hair sample, diameters were measured at 10 different locations distributed evenly along the length of the hair using a Nikon Eclipse 90i microscope and NIS-Elements AR v. 6 software. The average diameter of each hair sample was used to calculate an average cross-sectional area of the hair. Force–displacement curves were converted to stress–strain curves by dividing the force by the average cross-sectional area of the hair (assuming a circular cross section) and dividing the displacement by the nominal gauge length.

The hair strands were mounted on the tensile tester and the force required to extend the hair by a unit length (force versus extension) was collected. Measurements were taken to the point of mechanical failure, characterized by breaking of the hair. Stress–strain curves were obtained by normalizing the *y*-axis of the measured force versus extension curves by cross-sectional area of the hair sample (obtained from microscope images) and by normalizing the *x*-axis by the length of the hair. Three distinct regions were observed in stress–strain curves, as depicted in figure 10: (1) a linear regime at less than 10% extension, followed by (2) a plateau at ~10% up to~30% extension; and (3) above 30%, extension another linear regime is observed up to the point of failure [25]. The Young's modulus is obtained by obtaining the slope of the linear regime at low extension by a linear fit.

Using Kaleidagraph v. 4.03, the Young's modulus was determined by applying a linear curve fit to the initial linear region of

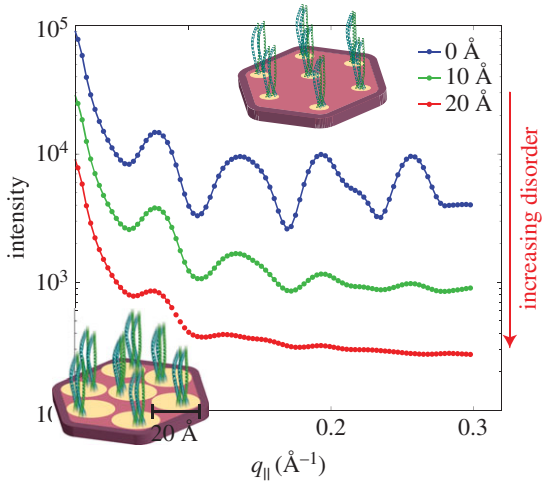

Figure 9. Calculated small-angle diffraction pattern. Intensity is plotted on a logarithmic scale such that higher-order reflections are better visible. Scattered intensity is plotted for displacement amplitudes of 0, 10 and 20 Å. The cartoons depict the results of calculations where the structure of the keratin bundles within a microfibril is modelled with increasing Debye–Waller Factor, assuming a hexagonal packing of keratin tetramers. Increasing DWF, or positional disorder, leads to decreased intensity for higher-order peaks. (Online version in colour.)

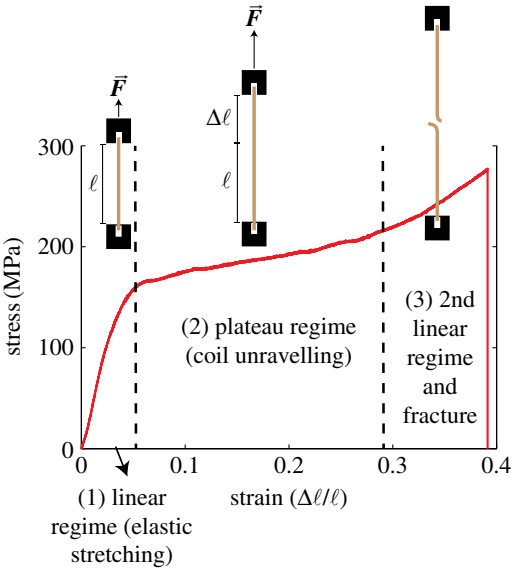

Figure 10. Typical stress–strain curve obtained from tensile tests. (1) An initial linear regime is observed, characterized by elastic stretching of the keratin proteins in the hair; (2) a plateau region is observed, when the coiled-coil α-keratin is pulled into a β-sheet configuration; and (3) a second linear regime is observed up to the point of hair fracture [16,17,22,25,26]. (Online version in colour.)

the stress–strain curve. Breaking stress was measured at the stress at failure and breaking strain was measured at the strain at failure. Owing to the strong and predictable effects of diameter on the mechanical properties of the hair fibres, diameter was included in the statistical model for these variables. Data for Young's modulus and breaking stress were ln-transformed to linearize their relationship to diameter. Effects of the GAN condition on all three material properties (Young's modulus, breaking stress and breaking strain) were calculated using an analysis of co-variance (ANCOVA) with diameter as a covariate using JMP statistical software (v. 12.2.0).

We note that the analysis in this paper is focused on the elastic modulus determined from the first linear regime, and the stress and strain at break. The plateau and second linear regime have

been attributed to the opening up of two distinctly different and well-defined portions of the monomer of the intermediate filament; the increased slope in the second linear region can be attributed to the influence of the sulfur bonds in one of the segments [25]. This global behaviour is the result of the complex hierarchical multi-scale interactions in human hair [27,28]. The entire stress–strain curve can be described by a general multi-scale approach for the mechanical behaviour of three-dimensional networks of macromolecules undergoing strain-induced unfolding [29].

Ethics. This research was approved by the Hamilton Integrated Research Ethics Board (HIREB) under approval number 14-474-T. Written consent was obtained from all participating adults, and informed consent was also obtained, in writing, from the next of kin on behalf of the children enrolled in the study.

Author's contributions. A.S., R.J.A., A.N., L.K., D.F., R.G. and M.C.R. conceived and designed experiments. A.S., R.J.A., A.N. and M.C.R. performed the experiments. A.S., R.J.A., A.N., D.F. and M.C.R. analysed the data. A.S., R.J.A., L.K., D.F., E.R.K., R.G. and M.C.R. contributed materials/reagents/analysis tools. A.S., R.J.A., L.K., D.F. and M.C.R. wrote the manuscript.

Competing interests. We declare we have no competing interests.

Funding. This research was funded by the Natural Sciences and Engineering Research Council of Canada (NSERC), the National Research Council Canada (NRC), the Canada Foundation for Innovation (CFI) and the Ontario Ministry of Economic Development and Innovation. R.J.A. is the recipient of an NSERC PGS-D. M.C.R. is the recipient of an Early Researcher Award of the Province of Ontario and a University Scholar Award from McMaster University. E.R.K. and R.G. are supported by the Hannah's Hope Fund and are grateful to Lori Sames for assistance.

References

1. Kretzschmar HA, Berg BO, Davis RL. 1987 Giant axonal neuropathy: a neuropathological study. *Acta Neuropathol.* **73**, 138–144. (doi:10.1007/BF00693779)
2. Johnson-Kerner BL, Roth L, Greene P, Wichterle H, Sproule DM. 2014 Giant axonal neuropathy: an updated perspective on its pathology and pathogenesis. *Muscle Nerve* **50**, 467–476. (doi:10.1002/mus.24321)
3. Engel A, Eichner R, Aebi U. 1985 Polymorphism of reconstituted human epidermal keratin filaments: determination of their mass-per-length and width by scanning transmission electron microscopy (stem). *J. Ultrastruct. Res.* **90**, 323–335. (doi:10.1016/S0022-5320(85)80010-1)
4. Fraser RD, Macrae TP. 1985 Structural implications of the equatorial X-ray diffraction pattern of α-keratin. *Biochim. Biophys. Acta* **29**, 229–240. (doi:10.1016/0006-3002(58)90179-3)
5. Briki F, Busson B, Doucet J. 1998 Organization of microfibrils in keratin fibers studied by X-ray scattering: modelling using the paracrystal concept. *Biochim. Biophys. Acta* **1429**, 57–68. (doi:10.1016/S0167-4838(98)00216-7)
6. Er Rafik M, Doucet J, Briki F. 2004 The intermediate filament architecture as determined by X-ray diffraction modeling of hard alpha-keratin. *Biophys. J.* **86**, 3893–3904. (doi:10.1529/biophysj.103.034694)
7. Robbins CR. 2012 *Chemical and physical behavior of human hair*, 5th edn. Berlin, Germany: Springer Berlin Heidelberg.
8. Zhang Y, Alsop RJ, Soomro A, Yang F-C, Rheinstädter MC. 2015 Effect of shampoo, conditioner and permanent waving on the molecular structure of human hair. *PeerJ* **3**, e1296. (doi:10.7717/peerj.1296)
9. Yang F-C, Zhang Y, Rheinstädter MC. 2014 The structure of people's hair. *PeerJ* **2**, e619. (doi:10.7717/peerj.619)
10. Alsop RJ, Soomro A, Zhang Y, Pieterse M, Fatona A, Dej K, Rheinstädter MC. 2016 Structural abnormalities in the hair of a patient with a novel ribosomopathy. *PLoS ONE***11**, e0149619. (doi:10.1371/journal.pone.0149619)
11. Yang F-C, Peters RD, Dies H, Rheinstädter MC. 2014 Hierarchical, self-similar structure in native squid pen. *Soft Matter* **10**, 5541–5549. (doi:10.1039/C4SM00301B)
12. Neukirch S, Goriely A, Hausrath AC. 2008 Chirality of coiled coils: elasticity matters. *Phys. Rev. Lett.* **100**, 038105. (doi:10.1103/PhysRevLett.100.038105)
13. Crick FHC. 1952 Is α-keratin a coiled coil? *Nature* **170**, 882–883. (doi:10.1038/170882b0)
14. Cohen C, Parry DA. 1994 α-helical coiled coils: more facts and better predictions. *Science* **263**, 488–489. (doi:10.1126/science.8290957)
15. Lupas AN, Gruber M. 2005 The structure of α-helical coiled coils. *Adv. Protein Chem.* **70**, 37–38. (10.1016/S0065-3233(05)70003-6)
16. Wortmann F-J, Zahn H. 1995 The stress/strain curve of α-keratin fibers and the structure of the intermediate filament. *Textile Res. J.* **64**, 737–743. (doi:10.1177/004051759406401206)
17. Kreplak L, Franbourg A, Briki F, Leroy F, Dalle D, Doucet J. 2002 A new deformation model of hard α-keratin fibers at the nanometer scale: implications for hard α-keratin intermediate filament mechanical properties. *Biophys. J.* **82**, 2265–2274. (doi:10.1016/S0006-3495(02)75572-0)
18. Astbury WT, Sisson WA. 1935 X-ray studies of the structure of hair: wool, and related fibres. III. The configuration of the keratin molecule and its orientation in the biological cell. *Proc. R. Soc. Lond. A* **150**, 533–551. (doi:10.1098/rspa.1935.0121)
19. Pauling L, Corey RB. 1951 The structure of hair, muscle, and related proteins. *Proc. Natl Acad. Sci. USA* **37**, 261–271. (doi:10.1073/pnas.37.5.261)
20. Fraser RD, MacRae TP, Rogers GE. 1962 Molecular organization in α-keratin. *Nature* **193**, 1052–1055. (doi:10.1038/1931052a0)
21. Guinier A. 1994 *X-ray diffraction in crystals, imperfect crystals, and amorphous bodies*. North Chelmsford, MA: Courier Corporation.
22. Kreplak L, Doucet J, Dumas P, Briki F. 2004 New aspects of the α-helix to β-sheet transition in stretched hard α-keratin fibers. *Biophys. J.* **87**, 640–647. (doi:10.1529/biophysj.103.036749)
23. Rebenfeld L, Weigmann HD, Dansizer C. 1966 Temperature dependence of the mechanical properties of human hair in relation to structure. *J. Soc. Cosmet. Chem.* **17**, 525–538.
24. Kim SN, Lee SY, Choi MH, Joo KM, Kim SH, Koh JS, Park WS. 2013 Characteristic features of ageing in korean women's hair and scalp. *Br. J. Dermatol.* **168**, 1215–1223. (doi:10.1111/bjd.12185)
25. Feughelman M. 1959 A two-phase structure for keratin fibers. *Textile Res. J.***29**, 223–228. (doi:10.1177/004051755902900305)
26. Chou C-C, Lepore E, Antonaci P, Pugno N, Buehler MJ. 2015 Mechanics of trichocyte α-keratin fibers: experiment, theory, and simulation. *J. Mat. Res.* **30**, 26–35. (doi:10.1557/jmr.2014.267)
27. Akkermans RLC, Warren PB. 2004 Multiscale modelling of human hair. *Phil. Trans. R. Soc. Lond. A* **362**, 1783–1793. (doi:10.1098/rsta.2004.1395)
28. Keten S, Buehler MJ. 2010 Nanostructure and molecular mechanics of spider dragline silk protein assemblies. *J. R. Soc. Interface* **7**, 1709–1721. (doi:10.1098/rsif.2010.0149)
29. De Tommasi D, Puglisi G, Saccomandi G. 2015 Multiscale mechanics of macromolecular materials with unfolding domains. *J. Mech. Phys. Solids* **78**, 154–172. (doi:10.1016/j.jmps.2015.02.002)